euronoise

A comparison of SONAH and IBEM for near-field acoustic holography

Peter Juhl[a] and Jesper Gomes[b]

[a]Institute of Sensors, Signals and Electrotechnics, University of Southern Denmark, Niels Bohrs Allé 1, 5230 Odense S, Denmark
[b]Brüel & Kjær Sound and Vibration Measurement A/S, Skodsborgvej 307, DK-2850 Nærum, Denmark
pmjuhl@sense.sdu.dk

Among the popular techniques for acoustic source identification in complex environments are the Statistically Optimal Near Acoustic Holography (SONAH) and the Inverse Boundary Element Method (IBEM). These two methods are quite different regarding the underlying assumptions and the practical implementations: Whereas SONAH performs the back-propagation of the sound field to a plane surface; the IBEM has no restrictions on the radiating geometry. On the other hand, IBEM requires the generation of a surface mesh and a time consuming solution process. The present paper compares the performance of the methods for a number of experimental test cases and studies the influence on the performance of the models when changing selected parameters.

1 Introduction

Today, several methods exist for calculating the velocity and/or sound pressure on a vibrating surface based on measurements of particle velocities or (more often) sound pressures at points outside the surface. If the measurement points are relatively close to the vibrating surface, the measurement is able to capture evanescent components of the radiated sound field, and the methods for reconstructing the surface velocity or pressure belong to the area of Near-field Acoustical Holography (NAH).

Methods of NAH can be placed in two groups: Several methods like the original NAH based on spacial Fourier transforms, the Statistically Optimized Near-field Acoustical Holography (SONAH) and the Helmholtz Equation Least-Squares (HELS) method are based on assumptions on the source geometry (i.e. planar, spherical or cylindrical) whereas methods like the Inverse Boundary Element Method (IBEM) and the Equivalent Source Method (ESM) can deal with general geometries.

However, a general method like the IBEM might not be the best choice in many situations. The primary strength of the IBEM is its ability to deal with general geometries, but the cost is that a discretized model of the structure is needed and that the calculation time typically is large compared to the other methods. Furthermore, in order to fully resolve the vibrational pattern of a structure, the measurement surface should *surround* the radiating surface, which often means that a complicated setup of microphones is needed. Therefore, it is sometimes desireable to use IBEM with microphone arrays designed for use with e.g. SONAH, i.e. microphones arranged in a fixed and regular planar grid. In these cases it turns up that the IBEM typically is able to reconstruct the vibrational pattern on the surfaces of the radiating structure, that is close to the measurment surface: surface vibrations of remote surfaces are associated with small singular values, and they are consequenly suppressed by the regularization.

In the present paper a microphone array of 8 by 8 regulary spaced microphones is used to reconstruct the surface velocity of a steel plate mounted in a rectangular box. Hence, that situation is well suited for the SONAH method, which therefore will be used as the benchmark test case.

Two Inverse Boundary Element Method strategies are considered. One method is based on a direct BEM formulation, which deals with the surface velocity and pressure directly, whereas the other is is an indirect method based on the Single Layer Formulation (SLF), that deals with a source distribution with no physical quantity directly associated.

2 Theory

All the methods considered work in the frequency domain and the time factor $e^{j\omega t}$, where ω is the angular frequency, will be supressed throughout the text. Hence, the governing differential equation for the sound pressure p is Helmholtz equation,

$$\nabla^2 p + k^2 p = 0, \tag{1}$$

where the wavenumber $k = \omega/c$, and c is the speed of sound.

The particle velocity in the direction $\mathbf{n}$ is related to the pressure through Euler's equation

$$v_n = \frac{-1}{j\omega\rho}\nabla p \cdot \mathbf{n}, \tag{2}$$

where ρ is the rest density of the fluid.

2.1 SONAH

In SONAH the key idea is to represent the sound pressure $\mathbf{p_F}$ in a given set of positions as the (infinite) sum of plane and evanescent waves of complex amplitudes $\mathbf{a}$ [1],

$$\mathbf{p_F} = \mathbf{A}\mathbf{a}. \tag{3}$$

Each column in the matrix $\mathbf{A}$ represents a plane or evanescent wave, and each row is the value of these wavefunctions at the measurement points. In the limit of an infinite number of waves, the number of columns of $\mathbf{A}$ and rows of $\mathbf{a}$ tend to infinity, and Eq (3) can not be solved directly. However, it can be shown [2] that an alternative formulation can be used to calculate the regularized solution for the sound pressure and particle velocity on the reconstruction plane. An important parameter of SONAH is the virtual source plane, at which the plane and evanescent waves have the same amplitude [2]. Previous studies have shown that a distance of about 1.5 microphone spacing (i.e. 4.5 cm) from the reconstruction surface is a good overall choice, and this value will be used in this study.

2.2 IBEM

The Helmholtz Integral Equation (HIE) establishes the relation between the pressure at a field point $p(P)$ and the pressure $p(Q)$ and the normal particle velocity $v_n(Q)$

on a surface S by an integral equation [3]:

$$C(P)p(P) = \int_S \left(\frac{\partial G(R)}{\partial n} p(Q) + \mathrm{j}\omega\rho G(R) v_n(Q) \right) \mathrm{d}S, \tag{4}$$

where the Green's function $G(R)$ is defined as

$$G(R) = G(|P-Q|) = \frac{\mathrm{e}^{-\mathrm{j}kR}}{4\pi R}. \tag{5}$$

The $C(P)$ factor is the ratio of the solid angle occupied by the fluid to 4π which results in $C(P) = 1$ for P's placed entirely in the fluid domain and $C(P) = 0.5$ if P is placed on a smooth surface [3]. In this work the HIE is discretized using linear quadrilateral elements resulting in a matrix relation between discretized (nodal) pressures $\mathbf{p_S}$ and normal velocities $\mathbf{v_S}$ on the surface S,

$$\mathbf{A}\mathbf{p_S} + \mathbf{B}\mathbf{v_S} = 0, \tag{6}$$

where the matrices $\mathbf{B}$ and $\mathbf{A}$ contain terms relating to surface integrals of Green's function and its normal derivative for collocation points placed at the nodal positions on the surface. (In $\mathbf{A}$ the $C(P)$ factors of the corresponding collocation point has been subtracted from the diagonal terms in accordance with Eq (4).)

Likewise a discretized version of Eq (4) can be obtained for field points:

$$\mathbf{p_F} = \mathbf{A^F}\mathbf{p_S} + \mathbf{B^F}\mathbf{v_S}, \tag{7}$$

where each row in the matrices $\mathbf{A^F}$ and $\mathbf{B^F}$ refers to integrating Eq (4) with respect to a position P in the fluid outside S.

Combining Eqs (6) and (7) results in

$$\mathbf{p_F} = (-\mathbf{A^F}(\mathbf{A}^{-1}\mathbf{B}) + \mathbf{B^F})\mathbf{v_S} = \mathbf{H}\mathbf{v_S}, \tag{8}$$

which establishes the desired relation between measured pressures and surface velocities.

2.3 ISLF

The Single Layer Formulation (SLF) is based on a distribution of simple sources (monopoles) on a surface S:

$$p(P) = \int_S G(R)\mu(Q)\mathrm{d}S, \tag{9}$$

where the Green's function is defined in Eq (5). Eq (9) directly relates pressures in the domain to a source distribution μ on the surface S, and if the same discretization scheme as for the BEM is used, the resulting matrix equation becomes,

$$\mathbf{p_F} = \mathbf{B^F}\mu, \tag{10}$$

where the matrix $\mathbf{B^F}$ of Eq (7) occurs again, since the kernel of Eq (9) is the same as the kernel of the second term in Eq (4). Hence, Eq (10) is the inverse problem to be solved for the unknown source distribution, but in order to arrive to a physical quantity such as the surface velocity, a relation between the regularized solution μ_λ and the surface velocity must be used,

$$v_{n_P}(P) = \mathrm{j}\omega\rho \int_S \frac{\partial G(R)}{\partial n_P} \mu_\lambda(Q)\ \mathrm{d}S + \frac{1}{2}\mu_\lambda(P), \tag{11}$$

which resembles the first term of the integral in Eq (4) execpt that the normal derivative is taken at the fixed point P instead of the running integration point Q. Hence, the discretized version of the regularized velocity $\mathbf{v}_\lambda$ may be computed as the matrix-vector product $\mathbf{v}_\lambda = \mathbf{A}^{n_P}\mu_\lambda$, where superscript n_P indicates that the normal is to be taken at P. For calculating the velocity at points in the fluid outside the surface,

$$v_{n_P}(P) = \mathrm{j}\omega\rho \int_S \frac{\partial G(R)}{\partial n_P} \mu_\lambda(Q)\ \mathrm{d}S, \tag{12}$$

must be used.

2.4 Regularization

The matrix equations in Eqs (8) and (10) are the discretized versions of the operators representing the relation between source terms and field pressures. The rapidly decaying nature of the near-field is reflected in an ill-conditioning of the coefficient matrices, and regularization is needed in order to obtain a meaningful solution. The Tikhonov regularized solution is found as the least squares solution of the equation on its standard form, i.e.

$$\mathbf{v}_\lambda = \mathbf{A}^{\#}_\lambda \mathbf{p} = (\mathbf{A}^H\mathbf{A} + \lambda^2\mathbf{I})^{-1}\mathbf{A}^H\mathbf{p}, \tag{13}$$

where λ is the regularization parameter, $\mathbf{I}$ is the identity matrix and superscript H denotes the Hermitian transpose [4]. Hence, an infinity of solutions exists depending on the choice of regularization parameter. The total performance of a method for inverse sound field calculations is a interaction between the sound field method (e.g. SONAH or IBEM) and the Parameter Choice Method (PCM). Several PCMs is discussed in the accompaning paper [2], and it was found that the Normalized Cumulative Periodogram (NCP) [5] worked well for the situation considered in the present work. Therefore, NCP is used as the PCM for all cases in the present paper. In general terms the NCP decides to include information (singular vectors) to the solution until the Fourier transform of the residual becomes as close to white noise as possible.

For SONAH the regularized solution for the sound pressure at $\mathbf{r}$, $p_\lambda(\mathbf{r})$ is

$$p_\lambda(\mathbf{r}) = \mathbf{p}^T(\mathbf{B}^H\mathbf{B} + \lambda^2\mathbf{I})^{-1}\mathbf{B}^H\alpha(\mathbf{r}), \tag{14}$$

where $\mathbf{B} = \mathbf{A}^H$, and $\alpha(\mathbf{r})$ is the vaules of the wave functions at $\mathbf{r}$ [2]. The velocity in a direction can be found using Eq (2) in Eq (14), which will affect the term $\mathbf{B}^H\alpha(\mathbf{r})$ only.

3 Experimental Results

A series of experiments were carried out in order to evaluate the methods considered. A 3-mm steel plate of dimensions 0.4 by 0.5 m was mounted using silicone as one face in a box of 19-mm MDF wood with the dimensions $0.4 \times 0.5 \times 0.4$ m. The plate was excited near the middle of the plate (at the position (0.18,0.19) m with random noise using a Brüel & Kjær exciter placed inside the box

and acting through a stinger and a Brüel & Kjær force transducer fastened to the plate using beeswax.

In order to establish a reference for the methods the normal velocity of the plate was measured in a grid of 16 × 14 points in the vertical and horizontal direction respectively using a Ometron laser vibrometer. The spacing between grid points was 0.03 m in both directions so that the measurement surface covered 0.39 × 0.45 m – i.e. almost the entire plate. Useful transfer functions between velocity and force was aquired using a Brüel & Kjær PULSE system in the frequency range of 100 - 3200 Hz (at very low frequencies noise dominated resulting in poor coherence).

At 3200 Hz the wavelength of sound waves in air is about 0.11 m and the wavelength of a travelling bending wave in the plate is about 0.09 m. The critical frequency is about 4000 Hz.

A 8x8 microphone array was placed in front of the plate at the distances 0.5, 1.5, 3.0, 4.5 cm. The spacing between microphones in the array was 3 cm in both directions and transfer functions between sound pressure and force was aquired using the PULSE system. For each distance four complementing positions of the array was combined to produce a measurement grid of 16 × 16 points in total. See Fig. 1 for a sketch of the setup.

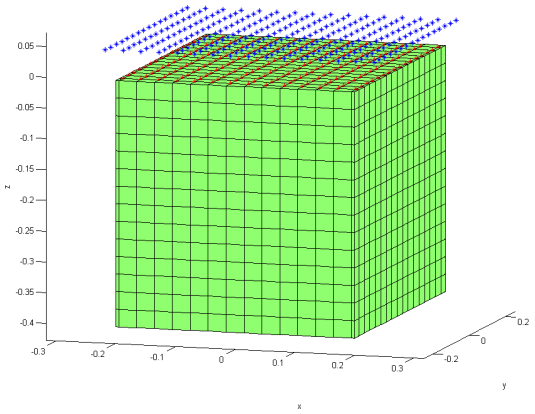

Figure 1: Sketch of the experimental setup. The box is shown with the BEM mesh used for the forward calculations. Measurement points for the vibrometer are indicated with red dots, and measurement points for the sound pressure are indicated with blue dots.

3.1 Forward Calculations

Initially a forward calculation from the measured velocities to field pressures is performed and compared to measured sound pressures in order to check the consistency of the measurements and of the models. For the calculations a direct collocation BEM is employed using linear quadrilateral elements - see Fig. 1. The mesh size of the BEM corresponds to the grid of measured velocities so the typical element size is 3 cm corresponding to an upper frequency of about 2.2 kHz if five elements per wavelength in air is required as a rule of thumb (empirically leading to an error of about 10 % or less). If five elements per structural wavelength is desired the upper frequency is about 1300 Hz. Fig. 2 shows the relative error calculated as the relative difference between the calculated and the measured sound pressures for the four distances. The error is calculated using the amplitude of the pressures only (discarding the phase), since the difference in phase response between microphones and laser vibrometer is unknown:

$$err = \frac{|| \, |\mathbf{p}_{BEM}| - |\mathbf{p}_{meas}| \, ||_2}{|| \, |\mathbf{p}_{meas}| \, ||_2}. \qquad (15)$$

It is seen that the error gradually increases from about 10 % at low frequencies to around 25 % at high frequencies. The error is significantly higher at certain frequencies which might be due poor signal to noise ratios at anti-resonances of the plate (for these frequencies the measured force in the denominator of the transfer function is at a minimum). Furthermore, the BEM employed for the forward calculation is known to suffer from the problem of non-uniqueness, which also might explain scattered outliers. For inverse problems the problem of non-uniqueness is less severe, since the near-singular nature of the coefficient matrix is dealt with during the regularization [6]. At very low frequencies (40 and 80 Hz) the error is large due to a poor signal from the laser vibrometer, and these two frequencies have been left out in the figures to follow.

In the frequency range where the BEM calculations can be trusted, the difference is generally less that 20 %.

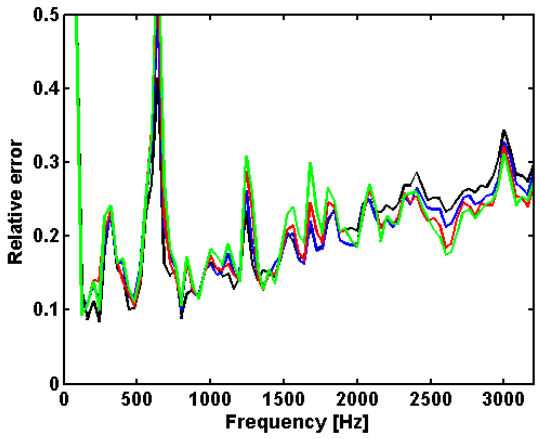

Figure 2: Relative difference between measured and calculated sound pressure for the four array distances. Black curve: 0.5 cm; blue curve: 1.5 cm; red curve: 3.0 cm; and green curve: 4.5 cm. The calculated sound pressures are based on measured velocities.

For the IBEM and the ISLF these error curves represent the best results one can hope for when using inverse calculations. At higher frequencies a finer mesh would probably increase the accuracy. The error can be explained as a combination of measurement error (e.g. noise) and modelling error (due to e.g. discretization). The assumption that only the steel plate vibrates might not be accurate and even though measurements has been carried out in an anechoic room, reflections occur from the structures supporting the box and the microphone array (each microphone is modelled as a point device). The SONAH has a quite different theoretical

basis and includes an infinity of plane and evanescent waves - hence, SONAH might or might not be able to perform source reconstruction with less error than found in Fig. 2.

3.2 Inverse calculations

The present case of a planar radiating surface and a parallel planar measurement microphone grid is very well suited for the SONAH algoritm. Therefore the SONAH calculations are used as a reference. In the accompaning paper [2] SONAH is used with different PCMs for the same experimental setup, and it was found that the reconstruction error of all PCMs studied was on about the same level. However, for reconstruction with the IBEM the NCP parameter choice method was favourable, and therefore the NCP is used as parameter choice method for all methods in the present paper.

In the figures to follow the relative error is shown as a function of frequency. The relative error is calculated as the norm of difference between measured and predicted velocity amplitudes normalized to the norm of the measured values – i.e. a similar error measure as introduced in Eq (15). In the error measure a grid of 12×16 measurement points (i.e. a total of 192 points) covering the surface of the steel plate was used in the residual and normalization vectors.

For almost all figures outliers can be observed. A few outliers probably occurs at anti-resonance frequencies of the plate, for which the measured force does not provide a good reference for the transfer functions, but generally outliers indicate that the combination of sound field calculation method and PCM did not result in a choice of regularisation parameter close to the optimal parameter.

3.2.1 SONAH

Fig. 3 shows the results produced by SONAH. It can be seen that the reconstruction error is generally low (10-25 %) at frequencies below 2000 Hz. Typically the error is smaller for array positions close to the box and there is a general tendency of an increase of error with frequency – a similar behavior was also found for the forward calculations (see Fig. 2). Generally the fluctuations of the curves are smaller for the distances of 0.5 cm and 1.5 cm than for the curves representing stand-off distances of 3.0 and 4.5 cm, which probably is due to the fact that the NCP does a better job in finding a near-optimal regularization paramater when the array is close to the box.

3.2.2 IBEM

The reconstruction errors for the four array stand off distances with IBEM are shown in Fig. 4. Generally the error increases with frequency from a level of 10-20 % at low frequencies to about 30-40 % at high frequencies. It is worth to notice that the best performance of the IBEM is obtained for a stand off distance of 4.5 cm. – i.e. the largest stand off distance. This result might be

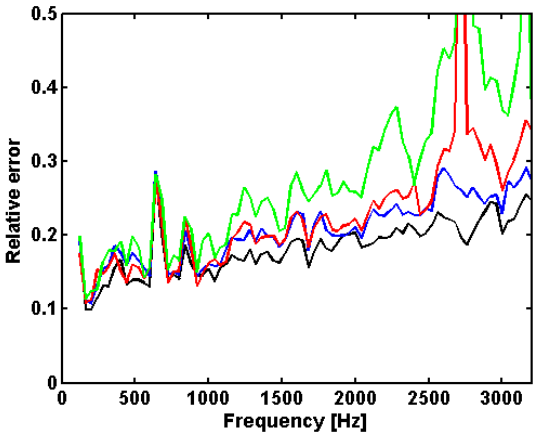

Figure 3: Relative difference between measured and calculated velocity for the four array distances using SONAH and NCP. Black curve: 0.5 cm; blue curve: 1.5 cm; red curve: 3.0 cm; and green curve: 4.5 cm. The virtual source distance is 4.5 cm (1.5 microphone spacing) larger than the physical distance

unexpected since the evanescent part of the sound field should be more difficult to reconstruct for a large stand off distance compared to a small stand off distance. The explaination for this behaviour is that the PCM fails to find a regularisation parameter close to the optimal when the measurement array is too close to the source [2].

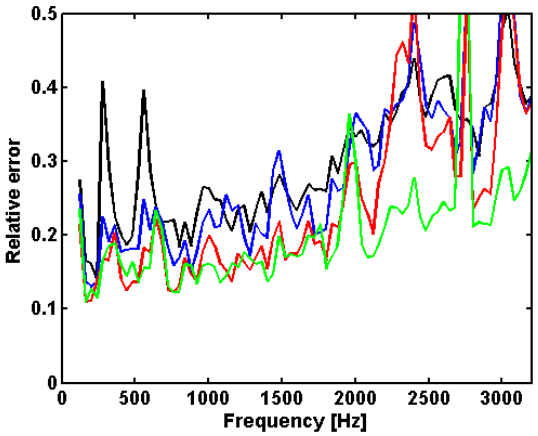

Figure 4: Relative difference between measured and calculated velocity for the four array distances using IBEM and NCP. Black curve: 0.5 cm; blue curve: 1.5 cm; red curve: 3.0 cm; and green curve: 4.5 cm.

3.2.3 ISLF

A similar behavior is observed with the Inverse Single Layer Formalation (see Fig. 5): The error increases with frequency and poor reconstruction is obtained for close array stand off distances. Generally the ISLF performs as good as the IBEM, and since that the computational work associated with the ISLF is less that with the IBEM, this method is favourable in the present test case.

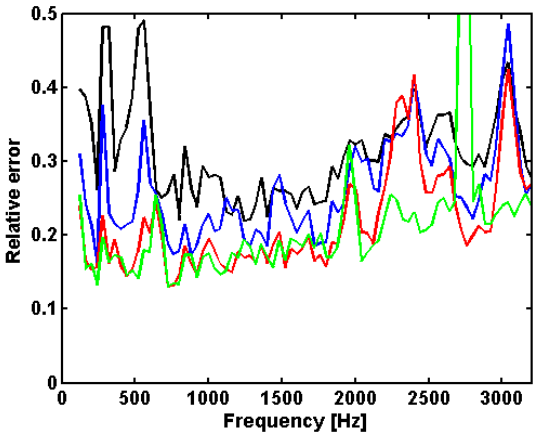

Figure 5: Relative difference between measured and calculated velocity for the four array distances using ISLF and NCP. Black curve: 0.5 cm; blue curve: 1.5 cm; red curve: 3.0 cm; and green curve: 4.5 cm.

3.2.4 Retracted ISLF

A main reason for the poor performance of the IBEM and the ISLF for array positions close to the surface of the box, is that the PCM fails in finding a regularization parameter, that is close to the optimal [2]. In the present situation it turns out that the solution is under-regularized - i.e. that the PCM choses a too small value for the regularization parameter. This indicates that the problem perhaps is too well-conditioned for the PCM to work as intended.

Inspired by the fact that SONAH works with a retracted virtual source plane, a Retracted Inverse Single Layer Formulation (RISLF) has been applied for the present problem. In the RSLF a virtual box is created at a larger distance to the measurement array than the physical box. A larger distance between the (virtual) source and the array makes the problem more ill-conditioned, which will trigger the PCM to choose higher values of the regularization parameter. The normal velocities on the reconstruction surface are then calculated from the regularized source density μ_λ by use of Eq (12).

Fig. 6 shows the relative error for a measurement distance of 0.5 cm, but with the virtual box placed 4.5 cm from the measurement plane. The error increases from about 10 % at low frequencies to about 20 % at high frequencies. It can also be noted the only minor fluctuations occur, which indicates that the PCM performs robustly for the present case.

4 Conclusions

Four methods of reconstructing the surface velocity of a vibrating object has been studied: the Statistically Optimized Near Acoustical Holography, the Inverse Boundary Element Method, the Inverse Single Layler Formulation and the Retracted Inverse Single Layer Formulation. All methods has been combined with Tikhonov regularization using the Normalized Cumulative Periodogram as the Parameter Choice Method. It was found that all methods were able to perform a reasonable reconstruction of the surface velocity for the experimental test case studied, but the combination of IBEM and ISLF with NCP lead to under regularizaton when the measurement array was close to the box. The RISLF performed very well for the latter situation.

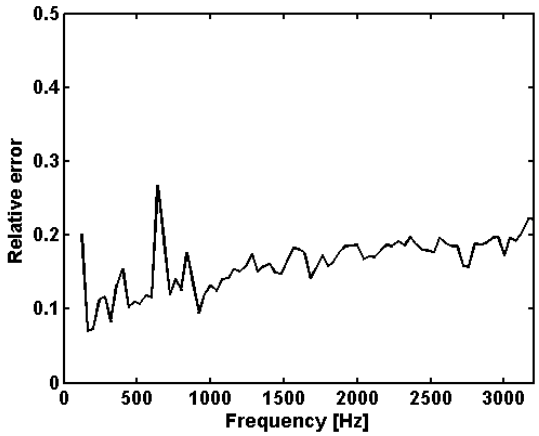

Figure 6: Relative difference between measured and calculated velocity for an array distance of 0.5 cm using Retracted ISLF and NCP. The virtual box is retracted 4.5 cm from the measurement array

References

[1] R. Steiner, J. Hald, "Near-field acoustical holography without the errors and limitations caused by the use of spatial DFT", *Int. J. Acoust. and Vib.* **6**, 83-89 (2001)

[2] J. Gomes, "A study on regularization parameter choice in near-field acoustical holography", *Proceedings Acoustics08*, CD-ROM (2008)

[3] P. Juhl, "The boundary element method for sound field calculations", *PhD thesis, The Acoustical Laboratory, Technical University of Denmark*, (1993)

[4] P. C. Hansen, "Rank-Deficient and Discrete Ill-Posed Problems: Numerical Aspects of Linear Inversion", *SIAM, Philadelphia* (1997)

[5] P. C. Hansen, M. Kilmer, R. H. Kjeldsen "Elploiting residual information in the parameter choice for discrete ill-posed problems", *BIT, Numer. Math.* **46**, 41-59 (2006)

[6] N. Valdivia, E. G. Williams, "Implicit methods of solution to integral formulations in boundary element method based nearfield acoustic holography", *J. Acoust. Soc. Am.*, 1559-1572 (2004)